Hyperfine level interactions of diamond nitrogen vacancy ensembles under transverse magnetic fields

Hannah Clevenson,[1,2,*] Edward H. Chen,[1,2] Florian Dolde,[1] Carson Teale,[1,2] Dirk Englund,[1] and Danielle Braje[2,†]

[1] *Department of Electrical Engineering and Computer Science, Massachusetts Institute of Technology, Cambridge, MA 02139, USA*
[2] *MIT Lincoln Laboratory, Lexington, MA 02420, USA*

(Dated: October 6, 2015)

We explore and characterize the behavior of ensembles of nitrogen vacancy qubits under transverse magnetic fields. In this regime, we predict and experimentally observe crossings and anti-crossings of the hyperfine splitting levels which occur at an order of magnitude less field than the axially-applied 510 G and 1000 G level anti-crossing characteristic of the excited and ground states. This system is a good candidate for electric field sensing, temperature sensing, and quantum memories in this novel transverse field regime. In addition, we quantify both advantages and limitations of addressing distributed ensembles of nitrogen vacancies in a bulk diamond under transverse magnetic field.

Nitrogen vacancy defect centers in diamond (NVs), are optically polarizable quantum systems with high-contrast spin-dependent fluorescence. Using electron spin resonance under ambient conditions, sensitivity to electric fields [1, 2], transverse and axial magnetic fields [3–8], temperature [9–12], strain [13] and pressure [14] have been observed via resonance frequency shifts of the NV ground-state manifold. When used as a sensor, non-separable sensitivity to multiple fields poses limitations. However, the Hamiltonian which governs the energy shifts can be tailored to enhance (or suppress) sensitivity to these external fields. Often touted for sensitivity to magnetic fields, NV energy level shifts are merely quadratic (*i.e.* zero to first order) in the strain-dominant, low magnetic field regime. An axial or transverse magnetic bias field ($B_{||}$ or $B_{\perp}$) lifts this degeneracy, energetically separating the spin states and increasing sensitivity to magnetic or electric fields, respectively. In this manuscript, we highlight an unexplored low-field regime where energy level splittings are on par with frequency shifts of the applied field. Here we account for both the electron and the nuclear spin of the ensemble, which reveals complex dynamics of nuclear spin state degeneracy and novel avoided level crossings. Note these features occur at low field as compared to the $B_{||} = 510$ G [15] and $B_{||} = 1000G$ [16] excited and ground state crossings, which have been used for nuclear spin polarization to decrease resonance line width and increase resonance contrast for increased sensitivity to shifts [17]. With exquisite agreement between theory and experiment, we paramaterize the regime where nuclear spin degeneracy and crossings occur and show utility toward sensing and quantum information applications.

In this paper, we examine a transverse-mangetic-field-dominant regime where $B_{\perp} \lesssim 100\,\mathrm{G}$ in the presence of small axial fields ($\lesssim 3\,\mathrm{G}$). The observed resonance frequency shifts are described by the following spin Hamiltonian of the ground triplet state in the presence of

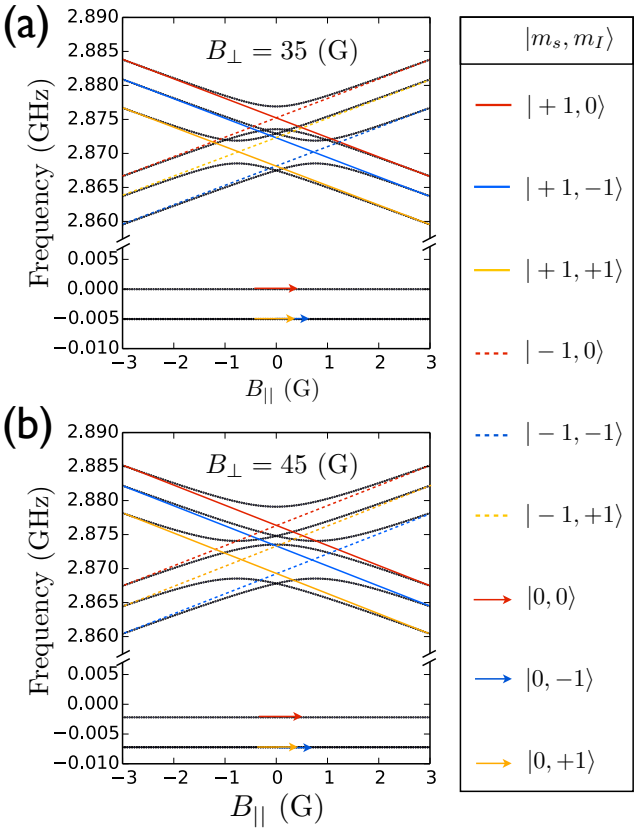

FIG. 1. Energy levels of the NV system with $B_{\perp} = 35\,\mathrm{G}$ and $B_{\perp} = 45\,\mathrm{G}$ assuming negligible strain and electric fields. The non-dressed electronic spin states are indicated with solid lines ($m_s = +1$), dashed lines($m_s = -1$), and arrows($m_s = 0$), while the non-dressed nuclear spin states are represented by the colors red ($m_I = 0$), blue ($m_I = -1$), and yellow ($m_I = +1$). Note $m_I = 0$ energy levels overlap the $m_I = \pm 1$ energy levels at lower transverse field as in (a), but not at higher fields (b).

* hannahac@mit.edu
† braje@ll.mit.edu

Distribution A: Public Release. The Lincoln Laboratory portion of this work is sponsored by the Assistant Secretary of Defense for Research & Engineering under Air Force Contract #FA8721-05-C-0002. Opinions, interpretations, conclusions and recommendations are those of the authors and are not necessarily endorsed by the United States Government.

magnetic, electric, and strain fields [18], taking into account the zero-field splitting, nuclear and electronic zeeman shifts, stark shifts, hyperfine splitting, and nuclear quadrupole effects:

$$\begin{aligned}\mathcal{H}_{gs} =&(D_{gs} + d_{||}\Pi_z)(S_z^2 - \frac{1}{3}S(S+1)) \\ &- d_\perp[\Pi_x(S_x^2 - S_y^2 + \Pi_y(S_xS_y + S_yS_x)] \\ &+ \beta[g_e(\vec{S}\cdot\vec{B}) - g_n(\vec{B}\cdot I)] \\ &+ A_{||}S_zI_z + A_\perp(S_xI_x + S_yI_y) + P_{gs}(I_z^2 - \frac{I^2}{3})\end{aligned} \quad (1)$$

where D_{gs} is the temperature-dependent ground state crystal field splitting, $d_\perp$ and $d_{||}$ are the components of the ground state electric dipole moment, the total effective electric field $\vec{\Pi} = \vec{E} + \vec{\sigma}$ encompasses both static electric and strain fields, g_e and g_n are the electric and nuclear Landé g-factors, $\beta \propto \mu_B$ is the Bohr magneton constant, $\vec{B}$ is the applied magnetic field, $A_{||}$ and $A_\perp$ are the axial and non-axial magnetic hyperfine tensors describing interactions with local nuclear spins, P_{gs} is the nuclear electric quadrupole parameter, and S_k is the spin projection onto the k axis with eigenvalues 0, $\pm\hbar$, corresponding to $m_s = 0, \pm 1$ [18]. Figure 1 shows the calculated energy levels as a function of axial field for a fixed transverse field.

Solving for the eigenvectors of this hamiltonian indicates that transverse magnetic fields induce state mixing. This state-mixing affects which transitions are allowed. For clarity, we neglect intrisnic strain as it is expected to be relatively low in type IIa diamond and plot energy levels as a function of axial field (Fig. 1). There are several interesting features to note. First, off-diagonal terms in the Hamiltonian cause the $m_s = \pm 1$ states to mix and cross each other when we seep a small applied axial field. This double electron spin flip anti-crossing occurs specifically as $m_s = +1$ states cross $m_s = -1$ states with identical nuclear spin [18].

Additionally, for transverse fields under $\sim$ 40 G, as show in Fig. 1(a), an additional avoided level crossing arises. The $m_I = 0$ levels cross the $m_I = \pm 1$ levels, resulting in further state mixing and an as-of-yet undescribed electron-nuclear spin flip anti-crossing. In Fig. 1, state-mixing-induced anti-crossings are seen when the black lines do not follow the solid and dashed colored lines, which represent the undressesd spin states. The strength of these avoided level crossing can be characterized by the deviation of the energy level from the bare-basis energy. Figure 2 depicts the strength of these splittings through a range of transverse fields.

As predicted in Ref. [18], the strength of the double electron spin flip anti-crossing, marked "E" in this figure, is proportional to $B_\perp^2$. These electron-spin anti-crossings are centered around $B_{||} = 0, \pm 0.75$ G. While this anti-crossing continues to increase in strength as $B_\perp$ increases, the second anti-crossing, indicated "N" in this figure, disappears around 40 G when the energy levels

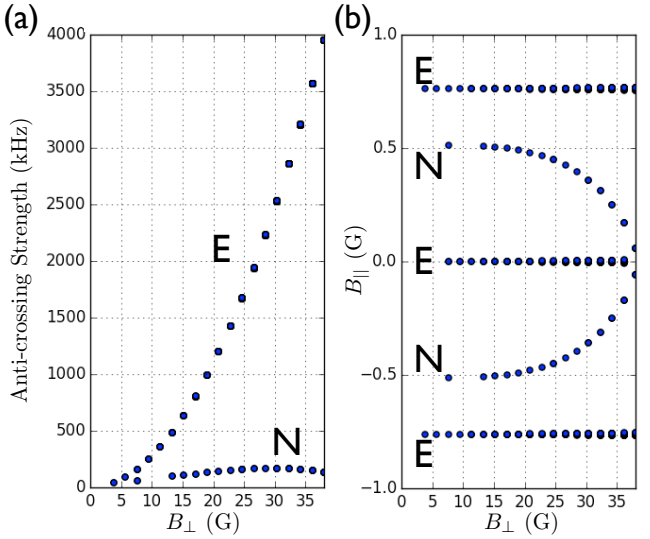

FIG. 2. (a) Anticrossing strength with increasing $B_\perp$. (b) Magnitude of small axial B fields at which the centers of these anti-crossings are observed. In both plots, the double electron spin flip anti-crossing is marked "E" and the electron-nuclear spin flip anti-crossing is marked "N". At fields greater than $B_\perp \sim 40$ G, anti-crossing "E" continues to increase quadratically and anti-crossing "N" goes to zero as the energy levels no longer overlap.

no longer overlap. The axial field about which this anti-crossing is centered decreases from roughly ± 0.5 G at $B_\perp = 15$ G to 0 G around $B_\perp \sim 40$ G. This is a direct result of the position of the $m_I = 0$ energy levels moving across the $m_I = \pm 1$ energy levels. The strength of this electron-nuclear spin flip anti-crossing peaks around 30 G.

While the Hamiltonian describes a single nitrogen vacancy, here we highlight the experimental-theory agreement for an ensemble of up to 10^{12} nitrogen vacancy centers equally distributed along the four diamond cyrstalographic axes using a light-trapping diamond waveguide geometry [19]. We lift the $m_s = \pm 1$ degeneracy by applying a static magnetic field and tune the microwave excitation to resonantly drive the $m_s = 0$ to $m_s = \pm 1$ spin transitions, causing a drop in the observed fluorescence. We assume that the intrinsic strain across the sample does not change over the course of the measurement and that observed shifts in the zero field splitting (ZFS) are caused by temperature or electric field changes. To apply transverse and axial magnetic fields, a 60 G permanent magnetic field (magnitude uniformity of 0.75% over a 2 cm^3 volume at the center) from a Halbach array is positioned around the sample. In addition, up to ± 30 G can be applied in $\pm$X, $\pm$Y, or $\pm$Z (lab frame) using Helmholtz coils. The four possible orientations of NV centers in the diamond lattice result in four sub-ensembles experiencing different combinations of transverse and axial fields. The high signal to noise ratio of this sample allows us to observe all four orientations in order to confirm the

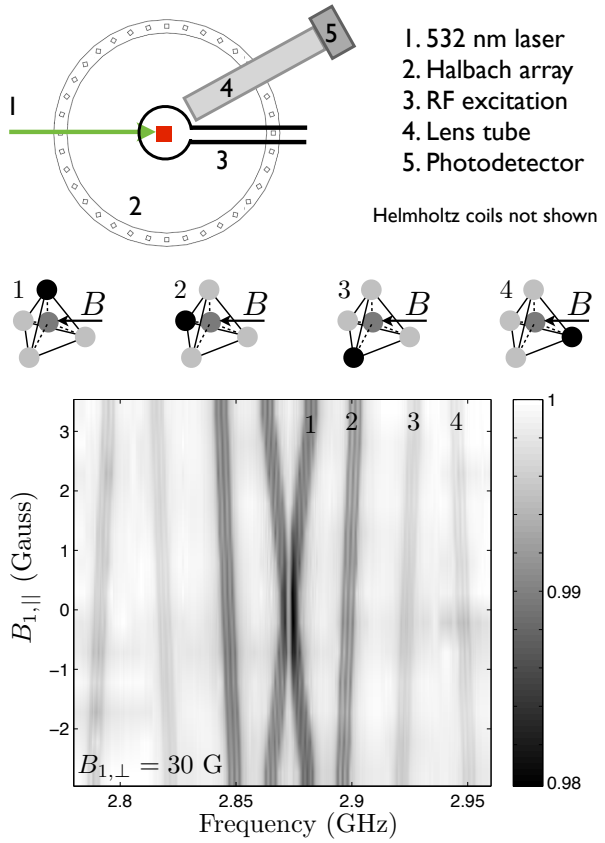

FIG. 3. Experimental setup. The diamond sample is located at the center of the concentric magnetic field sources and is provided with free-space green laser excitation and RF excitation. The fluorescence is collected with a silicon photodetector. The four orientations that make up the possible sub-ensembles of NV centers are shown with an applied magnetic field. An avoided crossing of $\sim$ 2.6 MHz is seen in sub-ensemble 1 when the perpendicular projection of the B field ($B_{1,\perp}$) is equal to 30 G and the axial projection of the B field onto the axis ($B_{1,||}$) is varied around zero field.

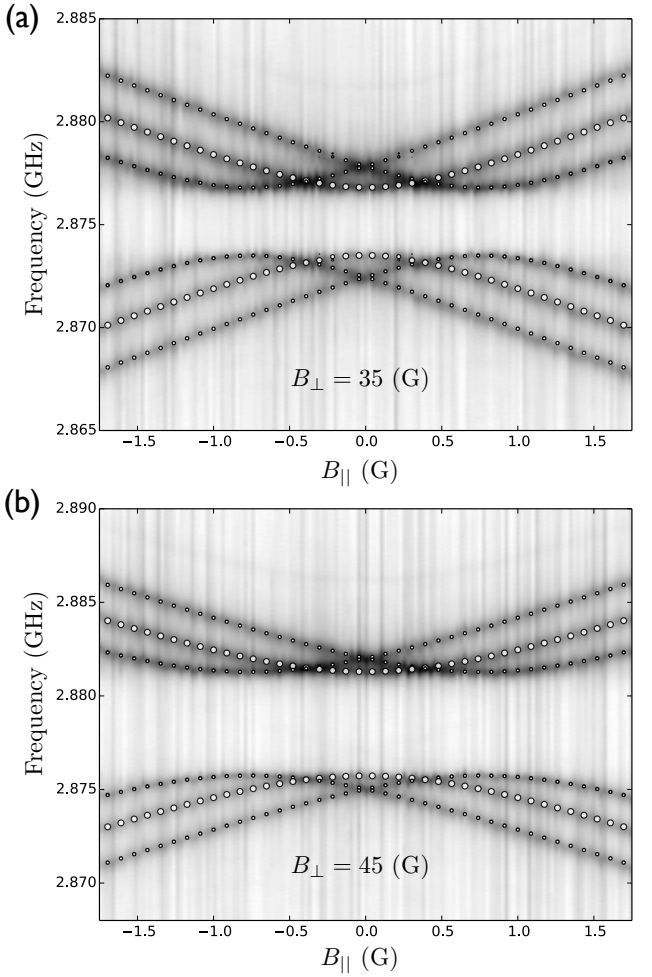

FIG. 4. Plots of transition energies as a function of axial field under fixed transverse field. Transitions for $B_\perp = 35$ G and $B_\perp = 45$ G are shown, which correspond to the energy levels in Fig. 1. Hyperfine interactions with nearby ^{13}C atoms are also visible.

orientation of the applied magnetic fields. We begin by aligning our total magnetic field to be perpendicular to one of the four orientations (Fig. 3) using the Helmholtz coils. Next, we apply a small axial field sweep in order to observe the anti-crossings in the electron spin resonance plots.

We examine the differences between the energy levels, or transition energies, which we can view using optically detected magnetic resonance (ODMR). Figure 4 overlays theory found by applying selection rules to the transitions seen in the energy levels in Fig. 1 over experimental data. The diameter of the circle corresponds to the probability of the transition. Two values of applied transverse field are shown, corresponding to the two values in Fig. 1. For both $B_\perp = 35$ G and $B_\perp = 45$ G, we see clear double-electron spin flip anti-crossings centered at $B_{||} = 0, \pm 0.75$ G (Fig. 2b) with anti-crossing strengths corresponding to those expected from Fig. 2a. As expected, we also see the zero-field splitting resonance increase with increased applied transverse field.

Concentrating on the region of interest at 30 G where the electron-nuclear spin flip anti-crossing is maximized, we increase the resolution of our scan and decrease the RF power to reduce power-broadening in our line widths (Fig. 5). The decreased RF power also results in a decrease in contrast and consequently a lower signal-to-noise ratio. However, we clearly observe the electron-nuclear spin flip anti-crossing at just under ± 0.4 G applied axial field as predicted by theory.

There are several ways that this moderate transverse magnetic field regime and the anti-crossings seen therein can impact diamond-based sensing. First, the double-electron spin anti-crossing suppresses sensitivity to changes in axial magnetic fields, which addresses an ongoing challenge in diamond-based sensing: decoupling the NV's sensitivity to its many environmental influences. As the applied transverse field is increased, the magni-

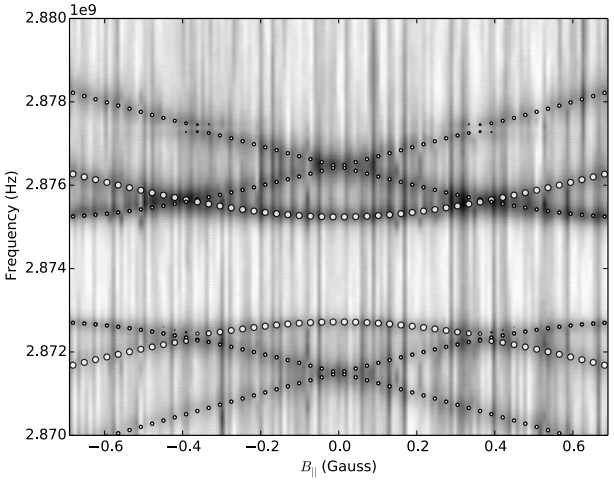

FIG. 5. Detail of double-electron and electron-nuclear spin anti-crossings at $B_\perp = 30$ G. The RF excitation power was reduced by 10 dB to reduce power broadening. This allows the higher resolution features to be observed, however it is at the expense of signal-to-noise-ratio. Double-electron spin anti-crossings of magnitude ~ 2.6 MHz are seen centered around $B_{||} = 0, \pm 0.75$ G and electron-nuclear spin anti-crossings of magnitude ~ 250 kHz are seen centered around $B_{||} = \pm 0.35$ G.

tude of this anti-crossing increases quadratically, increasing the magnitude of axial field to which the NV ensemble is insensitive.

Next, the double-electron spin anti-crossing causes the hyperfine transition levels to cross; at these crossings, we see increased signal contrast. In CW diamond-based sensing applications, the resonance contrast affects sensitivity linearly: doubling contrast doubles sensitivity. Furthermore, as this anti-crossing increases and the hyperfine transition levels are pressed closer together, all three levels can be effectively degenerate, providing a factor of three increase in sensitivity.

Additionally, in numerical simulations, both anti-crossings show a dependence on strain and electric field, paving the way for CW diamond-based strain and electric field sensing based on tracking the magnitude of this anti-crossing. This scheme would rely on being able to resolve the hyperfine transitions, as well as the high signal-to-noise ratio of the light-trapping diamond waveguide geometry. Furthermore, a simple method could be developed, based on the application of a transverse magnetic field in a low electric field environment, to characterize the intrinsic strain across a diamond sample.

Finally, we expect $\frac{dD_{gs}}{dT}$, the temperature dependence of D_{gs}, to decrease with increased transverse magnetic field [12]. Combining this advantage with the aforementioned increase in contrast results in a regime that is well-suited for temperature-stabilized measurements, relying on the ability to probe multiple sub-ensembles with different crystallographic projections of the applied transverse magnetic field. Comparing the sub-ensembles with known, varying dependences on temperature allows the temperature dependence term to fall out, further decoupling the diamond from its environment. This would be beneficial for the sensing of any other quantity.

The transverse magnetic fields may help overcome the influence of inhomogeneous strain present from diamond growth processes, a challenge in working with very large ensembles of NV centers. Combining this with insensitivity to small axial magnetic fields and potential insensitivity to temperature, the resultant system also presents itself as a strong candidate for a quantum memory. Transverse and axial magnetic fields could be used to read and write to the system, which is otherwise isolated from it's environment.

In conclusion, we have introduced, described, and observed double-electron spin and electron-nuclear spin anti-crossings in the diamond nitrogen vacancy system under transverse magnetic fields. These anti-crossings show potential for a variety of sensing applications. Similar increases in contrast can be achieved to the much higher, axially-applied 510 G and 1000 G level anti-crossings with much lower applied transverse fields. Furthermore, this unique regime allows selective decoupling of the NV from its environment, increasing it's appeal as both a sensor and a quantum memory.

[1] F. Dolde, H. Fedder, M. W. Doherty, T. Nobauer, F. Rempp, G. Balasubramanian, T. Wolf, F. Reinhard, L. C. L. Hollenberg, F. Jelezko, and J. Wrachtrup, Nat Phys **7**, 459 (2011).

[2] F. Dolde, M. W. Doherty, J. Michl, I. Jakobi, B. Naydenov, S. Pezzagna, J. Meijer, P. Neumann, F. Jelezko, N. B. Manson, and J. Wrachtrup, Phys. Rev. Lett. **112**, 097603 (2014).

[3] D. Budker and M. Romalis, Nature Physics **3**, 227 (2007).

[4] J. M. Taylor, P. Cappellaro, L. Childress, L. Jiang, D. Budker, P. R. Hemmer, A. Yacoby, R. Walsworth, and M. D. Lukin, Nature Physics **4**, 810 (2008).

[5] J. R. Maze, P. L. Stanwix, J. S. Hodges, S. Hong, J. M. Taylor, P. Cappellaro, L. Jiang, M. V. G. Dutt, E. Togan, a. S. Zibrov, a. Yacoby, R. L. Walsworth, and M. D. Lukin, Nature **455**, 644 (2008).

[6] G. Balasubramanian, I. Y. Chan, R. Kolesov, M. Al-Hmoud, J. Tisler, C. Shin, C. Kim, A. Wojcik, P. R. Hemmer, A. Krueger, T. Hanke, A. Leitenstorfer, R. Bratschitsch, F. Jelezko, and J. Wrachtrup, Nature **455**, 648 (2008).

[7] K. Fang, V. M. Acosta, C. Santori, Z. Huang, K. M. Itoh, H. Watanabe, S. Shikata, and R. G. Beausoleil, Phys. Rev. Lett. **110**, 130802 (2013).

[8] L. Rondin, J.-P. Tetienne, T. Hingant, J.-F. Roch, P. Maletinsky, and V. Jacques, Reports on Progress in

Physics **77**, 056503 (2014).
[9] G. Kucsko, P. C. Maurer, N. Y. Yao, M. Kubo, H. J. Noh, P. K. Lo, H. Park, and M. D. Lukin, Nature **500**, 54 (2013).
[10] D. M. Toyli, F. Charles, D. J. Christle, V. V. Dobrovitski, and D. D. Awschalom, Proceedings of the National Academy of Sciences **110**, 8417 (2013).
[11] P. Neumann, I. Jakobi, F. Dolde, C. Burk, R. Reuter, G. Waldherr, J. Honert, T. Wolf, A. Brunner, J. H. Shim, D. Suter, H. Sumiya, J. Isoya, and J. Wrachtrup, Nano Letters **13**, 2738 (2013).
[12] M. W. Doherty, V. M. Acosta, A. Jarmola, M. S. J. Barson, N. B. Manson, D. Budker, and L. C. L. Hollenberg, Phys. Rev. B **90**, 041201 (2014).
[13] P. Ovartchaiyapong, K. W. Lee, B. A. Myers, and A. C. B. Jayich, Nat Commun **5** (2014).
[14] M. W. Doherty, V. V. Struzhkin, D. A. Simpson, L. P. McGuinness, Y. Meng, A. Stacey, T. J. Karle, R. J. Hemley, N. B. Manson, L. C. L. Hollenberg, and S. Prawer, Phys. Rev. Lett. **112**, 047601 (2014).
[15] R. Fischer, A. Jarmola, P. Kehayias, and D. Budker, Phys. Rev. B **87**, 125207 (2013).
[16] R. J. Epstein, F. M. Mendoza, Y. K. Kato, and D. D. Awschalom, Nat Phys **1**, 94 (2005).
[17] A. Dréau, M. Lesik, L. Rondin, P. Spinicelli, O. Arcizet, J.-F. Roch, and V. Jacques, Phys. Rev. B **84**, 195204 (2011).
[18] M. W. Doherty, F. Dolde, H. Fedder, F. Jelezko, J. Wrachtrup, N. B. Manson, and L. C. L. Hollenberg, Phys. Rev. B **85**, 205203 (2012).
[19] H. Clevenson, M. E. Trusheim, C. Teale, T. Schroder, D. Braje, and D. Englund, Nat Phys **11**, 393 (2015).

ACKNOWLEDGEMENTS

The authors would like to thank L. Pham, M. E. Trusheim, and T. Schroder for helpful discussion. The Lincoln Laboratory portion of this work is sponsored by the Assistant Secretary of Defense for Research & Engineering under Air Force Contract #FA8721-05-C-0002 and the Office of Naval Research Section 321MS. Opinions, interpretations, conclusions and recommendations are those of the authors and are not necessarily endorsed by the United States Government. H. C. and E. H. C. are supported by the NASA Office of the Chief Technologist's Space Technology Research Fellowship.